JOURNAL OF MAGNETIC RESONANCE **124,** 20–34 (1997)
ARTICLE NO. MN967492

Time-Domain Quantification of Amplitude, Chemical Shift, Apparent Relaxation Time T_2^*, and Phase by Wavelet-Transform Analysis. Application to Biomedical Magnetic Resonance Spectroscopy

HACENE SERRAI,* LOTFI SENHADJI,† JACQUES D. DE CERTAINES,* AND JEAN LOUIS COATRIEUX†

Laboratoire de Résonance Magnétique en Biologie et Médecine, Faculté de Médecine, Université de Rennes, F-35043 Rennes Cedex, France; and †L.T.S.I., INSERM, CJF 93-04, Campus Scientifique de Beaulieu, F-35042 Rennes Cedex, France

Received April 23, 1996; revised September 24, 1996

The wavelet-transform method is used to quantify the magnetic resonance spectroscopy (MRS) parameters: chemical shift, apparent relaxation time T_2^*, resonance amplitude, and phase. Wavelet transformation is a time-frequency representation which separates each component from the FID, then successively quantifies it and subtracts it from the raw signal. Two iterative procedures have been developed. They have been combined with a nonlinear regression analysis method and tested on both simulated and real sets of biomedical MRS data selected with respect to the main problems usually encountered in quantifying biomedical MRS, specifically "chemical noise," resulting from overlapping resonances, and baseline distortion. The results indicate that the wavelet-transform method can provide efficient and accurate quantification of MRS data. © 1997 Academic Press

INTRODUCTION

The wavelet-transform method (WT), as proposed by Grossmann and Morlet (*1*), analyzes a nonstationary signal by transforming its input time domain into a time-frequency domain. Through translation and dilation operations, WT decomposes the signal according to a set of functions, all deduced from a unique prototype called a wavelet, assumed to be well localized both in time and frequency domains. Such a time-frequency representation could provide a more efficient solution than the usual Fourier-transform (FT) or other methods presently available to process MRS data (*2–5*).

WT is presented here as a quantification method in biomedical MRS with special attention to the FID signal characteristics. The FID signal, considered as a sum of damped sinusoids, is analyzed by WT and decomposed into its different components. The components are then successively separated with respect to their time durations and resonance frequencies, quantified, and subtracted from the raw signal. Chemical-shift and phase values are estimated from the WT phase information, while the WT modulus is used to estimate the values of the amplitude resonance A and the apparent relaxation time T_2^*. The problems often encountered in biomedical MRS applications, such as low signal-to-noise ratio, broad resonances, and ''chemical noise,'' can then be reduced, and accurate estimates of MRS parameter values may be obtained.

Two iterative procedures obtained from the application of WT to noise-free MRS signals composed of one and two resonances, respectively, are tested on simulated and real biomedical MRS data. The case of noisy signals is considered, and a classical solution is proposed.

CONTINUOUS WAVELET TRANSFORM

Let $L^2(R)$ be the vector space of square integrable functions, i.e., signals of finite energy. For $u(t)$ and $v(t)$ belonging to $L^2(R)$, the scalar product between u and v is given by

$$\langle u, v \rangle = \int u(t) v^*(t) dt, \qquad [1]$$

where the asterisk denotes the complex conjugate. For any function $u(t)$ of $L^2(R)$, $\hat{u}(\omega)$ is the associated Fourier transform defined by

$$\hat{u}(\omega) = \int_{-\infty}^{+\infty} u(t) e^{-i\omega t} dt. \qquad [2]$$

Any function $g(t)$ belonging to $L^2(R)$ is called an analyzing wavelet if it complies with the so-called admissibility condition (*6*):

$$C_g = \int_{-\infty}^{+\infty} \frac{|\hat{g}(\omega)|^2}{|\omega|} d\omega < \infty. \qquad [3]$$

With respect to this wavelet, the continuous wavelet transform of a signal $s(t)$ of finite energy is given by

1090-7807/97 $25.00

$$S_a(b) = \langle s, g_{a,b} \rangle = \frac{1}{a} \int s(t) g^* \left(\frac{t-b}{a} \right) dt \quad [4]$$

with

$$g_{a,b}(t) = \frac{1}{a} g\left(\frac{t-b}{a} \right), \; a > 0, \; b \in \mathrm{R}.$$

The transform maps the signal via a two-dimensional function on the time-scale domain plane (a, b). This operation is equivalent to a particular filter-bank analysis in which the relative frequency band widths are constant and related to the parameters a and b (scale parameter and translation parameter) and to the frequency properties of the wavelet g. $S_a(b)$ can be written as

$$S_a(b) = \int s(t) \tilde{g}_a(b-t) dt, \quad [5]$$

where $\tilde{g}_a(\cdot) = (1/a) g^*(- \cdot /a)$ is the impulse response of the filter.

There is a large set of functions satisfying the condition of Eq. [3]: not only can the analyzing wavelet be selected according to the signal features but the parameters a and b can be adjusted without limiting their range values. Transient events in a specific frequency domain can then be easily targeted. In practice, to achieve satisfactory signal analysis, regularity and a suitable time-frequency band-width product are required for g. The most commonly used analyzing wavelet has been the so-called Morlet wavelet defined by

$$g(t) = e^{-t^2/2} e^{i\omega_0 t} + c(t), \quad [6]$$

where $c(t)$ is a correction term to ensure that the admissibility condition is met. For $\omega_0 > 5$, the term $c(t)$ is negligible and $g(t)$ is practically applicable, where $\hat{g}(\omega) \approx 0$ if $\omega \leqslant 0$ (*7*). In the next section, the concept of the wavelet transform, briefly reviewed here, is considered in MRS signal analysis and quantification.

DEVELOPMENT OF A METHOD FOR MRS SIGNAL PROCESSING

Quantification is a necessary step for clinical implementation of large-scale MRS. Wavelet transform would appear to be an alternative method to the traditional FT for MRS data quantification. Referring to (*8*), the FID, considered here as a noise-free signal, is composed of a sum of damped complex sinusoids decaying with time and may be written as

$$s(t) = \sum_{j=1}^{N} A_j e^{(-t/T_{2_j}^*)} e^{i(\omega_j t + \varphi_j)} = \sum_{j=1}^{N} s_j(t), \quad [7]$$

where A_j, $T_{2_j}^*$, $\omega_j = 2\pi\delta_j$, and φ_j are the resonance amplitude, apparent relaxation time, angular frequency (chemical shift δ_j), and phase, respectively, of the component s_j. N denotes the total number of the signal resonances. We assume here, as is generally true, that the damping factor of each component, given by $1/\pi T_{2_j}^*$, is very small compared with ω_j.

Case of a Signal with One Component

According to Eq. [7], the FID signal may be written as

$$s(t) = A e^{(-t/T_2^*)} e^{i(\omega_s t + \varphi)} \quad [8]$$

Our aim is to estimate the values of the MRS parameters. Due to the causality of the FID signal, our conventions (a, $b \in R^+ \times R^+$) for the time-frequency domain display (Fig. 1) are the same as in (*9*).

According to Eq. [4], the WT of $s(t)$ with respect to the Morlet wavelet is given by

$$S_a(b) = \frac{1}{a} \int_0^{+\infty} A e^{(-t/T_2^*)} e^{i(\omega_s t + \varphi)} e^{\{-[(t-b)/a]^2/2\}} e^{-i\omega_0[(t-b)/a]} dt \quad [9]$$

Substituting u for $(t-b)/a$, $S_a(b)$ becomes

$$\begin{aligned} S_a(b) &= A e^{(-b/T_2^*)} e^{i(\omega_s b + \varphi)} \\ &\quad \times \int_{-b/a}^{\infty} e^{(-au/T_2^*)} e^{i(a\omega_s - \omega_0)u} e^{(-u^2/2)} du \\ &= s(b) \times J. \end{aligned} \quad [10]$$

Taking Δ as

$$\Delta = a\omega_s - \omega_0, \quad [11]$$

one can show that the quantity J, given by $\int_{-b/a}^{\infty} e^{(-au/T_2^*)} e^{i\Delta u} e^{(-u^2/2)} du$, is equivalent to

$$\begin{aligned} J &= e^{(1/2)(a/T_2^*)^2} e^{[-i\Delta(a/T_2^*)]} \int_{\alpha}^{\infty} e^{[(-t^2/2)+i\Delta t]} dt \\ &= e^{(1/2)(a/T_2^*)^2} e^{[-i\Delta(a/T_2^*)]} I \end{aligned} \quad [12]$$

with $\alpha = [(a/T_2^*) - (b/a)]$. If I is given the value shown in Appendix 1, the expression for $S_a(b)$ becomes

$$S_a(b) = s(b) e^{(1/2)(a/T_2^*)^2} e^{[-i\Delta(a/T_2^*)]} [B + iC]. \quad [13]$$

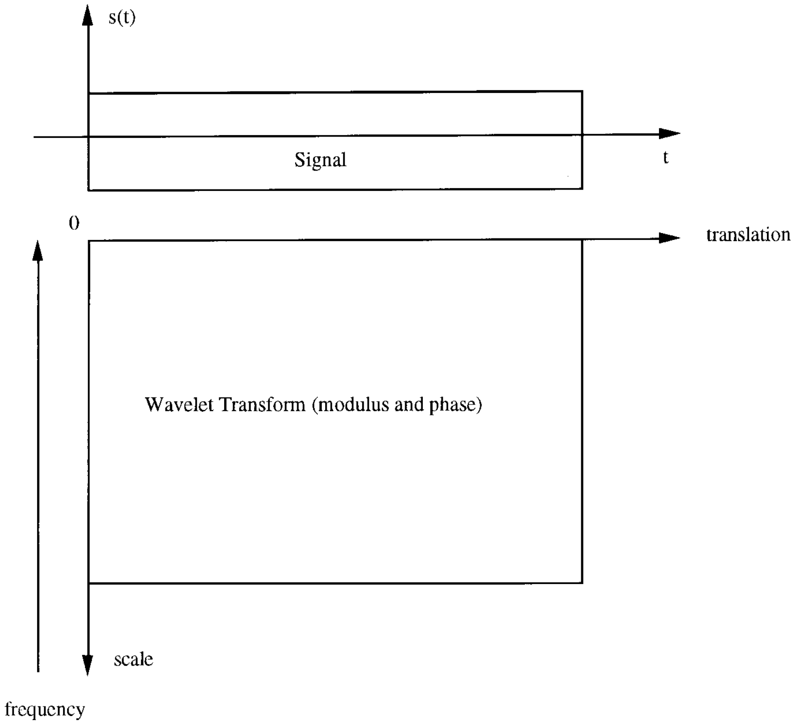

FIG. 1. Conventional representation of the wavelet-transform analysis as signal transforming functions in the time–frequency plane. Scale and translation are the two wavelet variables. The signal is represented through translation and scale operations from the time domain to a time-scale domain.

The terms B and C are the result of bordering effects of the projection of the signal onto the quart plane H along the axis where $b = 0$.

If we represent the result of the WT of Eq. [13] in terms of modulus and phase, we obtain

$$S_a(b) = |S_a(b)|e^{i\Phi_a(b)}. \qquad [14]$$

The modulus contains A and T_2^* and is given by

$$|S_a(b)| = Ae^{[(a^2/2T_2^{*2})-(b/T_2^*)]}\sqrt{B^2 + C^2}. \qquad [15]$$

The phase of $S_a(b)$, determined by ω and φ of the signal, is given by

$$\Phi_a(b) = \omega_s b + \varphi - \Delta\frac{a}{T_2^*} + \operatorname{arctg}\frac{C}{B}. \qquad [16]$$

Because of the presence of terms B and C in both the modulus and the phase, it is difficult to compute the values of the MRS parameters.

However, if $\Delta = 0$, the term C is null (see Appendix 1), and the phase $\Phi_a(b)$ in Eq. [16] becomes equal to the phase of the signal. This condition is fulfilled if ω_s is known. Unfortunately, this is not usually true. One can estimate the value of ω_s and approach $\Delta = 0$ by the following procedure. Let us take the two first terms of the series U_k in Appendix 1. The term B is restricted to

$$B = \sqrt{\frac{\pi}{2}}\,e^{(-\Delta^2/2)} \mp \sqrt{\frac{\pi}{2}}\sqrt{1 - e^{-\alpha^2}} \qquad [17]$$

and C becomes

$$C = \pm\sqrt{\frac{\pi}{2}}\,e^{-\Delta^2/2}(\sqrt{e^{\Delta^2}} - 1) - \Delta(1 - e^{-\alpha^2/2}). \qquad [18]$$

The signs $\mp$ in Eq. [17] and $\pm$ in Eq. [18] are conditioned by the signs of α and Δ respectively.

Consider now $\Omega_a(b) = d\Phi_a(b)/db$ as the instantaneous frequency of $S_a(b)$. Combining Eqs. [16], [17], and [18], $\Omega_a(b)$ may be written as

$$\Omega_a(b) = \frac{d\Phi_a(b)}{db} = \omega_s + \frac{d[\operatorname{arctg}(C/B)]}{db}. \qquad [19]$$

For a given value of the dilation parameter a of the wavelet, termed a_0, a value of the translation parameter b exists, termed b_r, such that for any $b > b_r$, the term $d[\operatorname{arctg}(C/B)]/db$ in Eq. [19] is negligible (see Appendix 2). A first estimation of ω_s is then obtained from

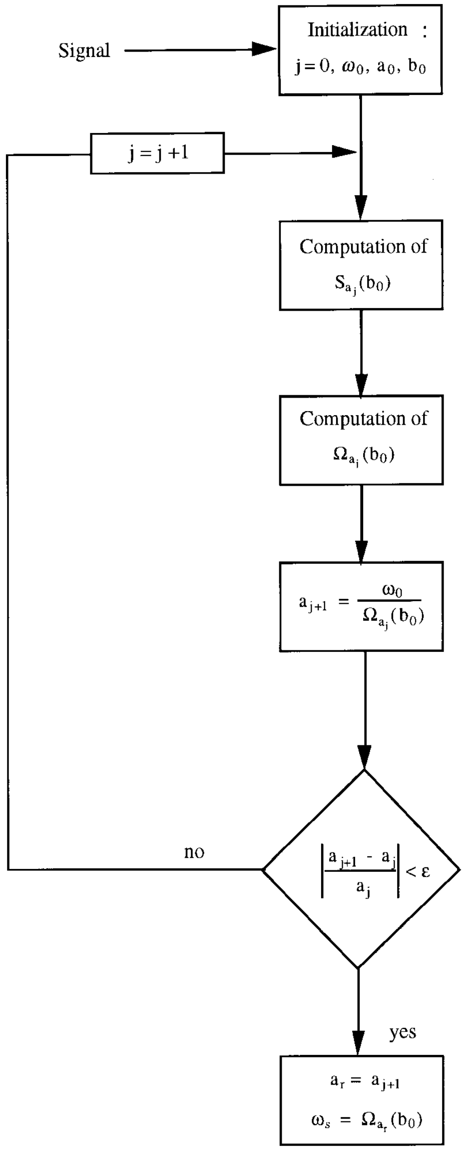

FIG. 2. First iterative-procedure flow chart to estimate the frequency-component values.

$$\Omega_{a_0}(b_0) \approx \omega_s \quad b_0 > b_r. \qquad [20]$$

The value of the translation parameter b_0 indicates that ω_s is estimated at the end of the FID signal, i.e., for the last points of the corresponding sampled signal.

To have more precision in the estimated value of ω_s, Δ should be closer to zero. In practice, this is obtained iteratively as follows (Fig. 2): $\Omega_{a_0}(b_0)$ is substituted for ω_s in Eq. [11] and Δ is assumed to equal zero. The new value a_1 of the dilation parameter is computed by

$$a_1 = \frac{\omega_0}{\Omega_{a_0}(b_0)}. \qquad [21]$$

The new calculated value of the instantaneous frequency $\Omega_{a_1}(b_0)$ associated with $S_{a_1}(b_0)$ is closer to ω_s. The iterative procedure converges after several iterations, when the following condition is fulfilled:

$$\left|\frac{a_{j+1} - a_j}{a_j}\right| < \epsilon, \qquad [22]$$

where a_j is the value of the dilation parameter obtained at the iteration j. ϵ is an arbitrarily small fixed positive number.

Once this first iterative procedure converges, the value of ω_s is estimated from $\Omega_{a_r}(b_0)$, where a_r is the final value of the dilation parameter a at convergence. Δ approaches zero, and this automatically implies that C decreases to zero and that B is restricted to $\sqrt{\pi/2}[1 \mp \sqrt{1 - e^{-\alpha^2}}]$. Consequently, $S_{a_r}(b)$ becomes

$$S_{a_r}(b) = \sqrt{\frac{\pi}{2}}\, e^{(1/2)(a_r/T_2^*)^2} \times [1 \mp \sqrt{(1 - e^{-\alpha^2})}]Ae^{(-b/T_2^*)}e^{i(\omega_s b + \varphi)}. \qquad [23]$$

The phase φ of the FID signal is directly estimated from the phase of $S_{a_r}(b)$, and a simple nonlinear regression algorithm (*14–16*) applied to the modulus gives the estimated values of A and T_2^*. $S_{a_r}(b)$ is now equal to the signal at every point $t = b$ up to a known function $F(b)$ given by

$$F(b) = \sqrt{\frac{\pi}{2}}\, e^{(1/2)(a_r/T_2^*)^2}[1 \mp \sqrt{(1 - e^{-\alpha^2})}]. \qquad [24]$$

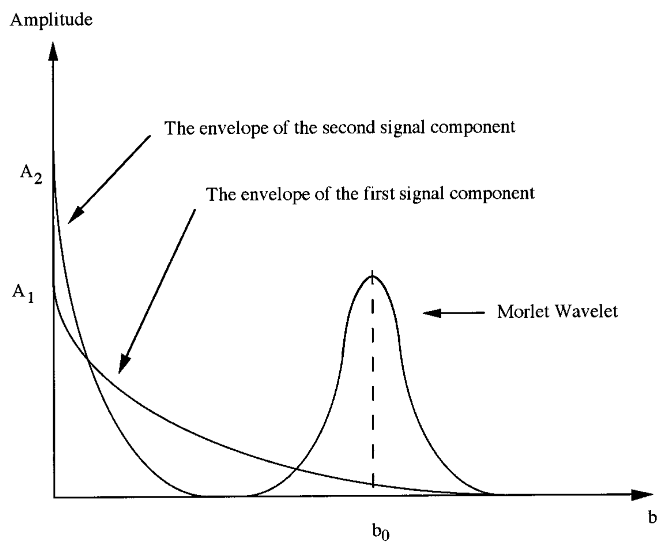

FIG. 3. Detection and estimation of the frequency of the longest-time component. The wavelet is translated to the end of the signal.

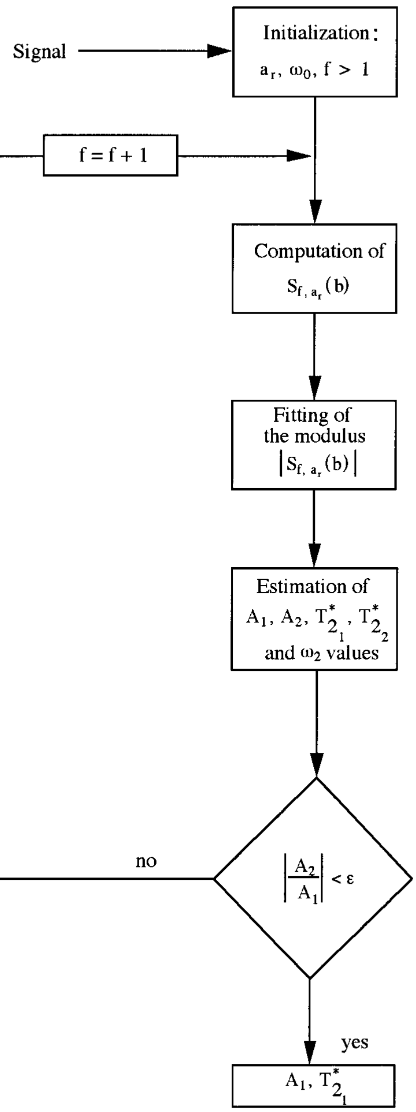

FIG. 4. Second iterative procedure steps to estimate A and T_2^* values.

Case of a Signal Composed of More Than One Component

The previous development allows us to generalize the procedure to a noise-free signal composed of more than one component. Let $s(t)$ be a FID signal composed of two resonances, given by

$$s(t) = A_1 e^{(-t/T^*_{2_1})} e^{i(\omega_1 t+\varphi_1)} + A_2 e^{(-t/T^*_{2_2})} e^{i(\omega_2 t+\varphi_2)}$$
$$= s_1(t) + s_2(t). \quad [25]$$

The WT of $s(t)$ with respect to the Morlet wavelet is

$$S_a(b) = \frac{1}{a}\int_0^\infty e^{\{-[(t-b)/a]^2/2\}} e^{-i\omega_0[(t-b)/a]} \times [A_1 e^{(-t/T^*_{2_1})} e^{i(\omega_1 t+\varphi_1)} + A_2 e^{(-t/T^*_{2_2})} e^{i(\omega_2 t+\varphi_2)}]\,dt. \quad [26]$$

Following the same procedure as for one component, we obtain

$$S_a(b) = |S1_a(b)|e^{i\Phi 1_a(b)} + |S2_a(b)|e^{i\Phi 2_a(b)}. \quad [27]$$

This representation of $s(t)$ is considered as a sum of two wavelet transforms, each one associated with one particular component of the signal and described as in Eq. [14] by its modulus and phase. The WT must be adapted to this type of signal in order to isolate the components from the FID and to estimate their MRS parameter values.

If we write Eq. [27] according to the WT associated with the first component s_1, we obtain

$$S_a(b) = |S1_a(b)|e^{i\Phi 1_a(b)}[1 + Z_a(b)e^{i\Theta_a(b)}]. \quad [28]$$

The interference terms resulting from the interactions between the two components are represented by $Z_a(b)$, where

$$Z_a(b) = \frac{|S2_a(b)|}{|S1_a(b)|} \quad [29]$$

and by $\Theta_a(b)$, which is equal to

$$\Theta_a(b) = \Phi 2_a(b) - \Phi 1_a(b). \quad [30]$$

If we substitute Eqs. [15] and [16] for the moduli and phases in Eqs. [29] and [30] respectively, we notice that the extent of interaction between the components depends particularly on the ratio A_2/A_1 and the difference $\omega_2 - \omega_1$.

Suppose now that the first component s_1 decays more slowly than the second component ($T^*_{2_1} > T^*_{2_2}$) (Fig. 3). For a given translation parameter value b of the wavelet, designated as b_r, the remaining component in the signal for any $b > b_r$ is the first component. WT of $s(t)$ is reduced to

$$S_a(b) = |S1_a(b)|e^{i\Phi 1_a(b)} \; b > b_r. \quad [31]$$

By comparing Eq. [31] and Eq. [28], the quantity $Z_a(b)e^{i\Theta_a(b)}$, describing the component interactions, becomes negligible for $b > b_r$. This allows us to use the iterative procedure described above to estimate the value of ω_1 and to compute a_r, i.e., the final value of the dilation parameter fulfilling Eq. [22]. At the convergence of the iterative procedure, the frequency of the component having the greatest apparent relaxation time value T_2^* is localized at the wavelet parameter values $b > b_r$ and $a = a_r$. As a result, according to Eq. [23] the corresponding WT is given by

$$S_{a_r}(b) = \sqrt{\frac{\pi}{2}} e^{(1/2)(a_r/T^*_{2_1})^2}[1 \mp \sqrt{(1 - e^{-\alpha_1^2})}] \times A_1 e^{(-b/T^*_{2_1})} e^{i(\omega_1 b+\varphi_1)} \; b > b_r. \quad [32]$$

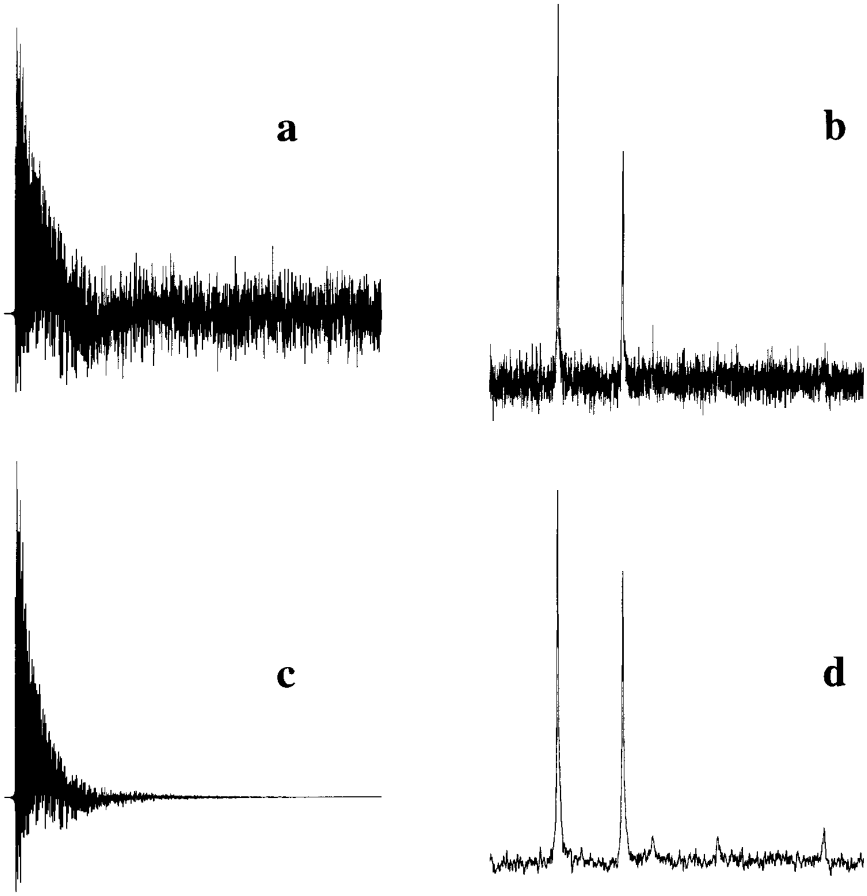

FIG. 5. Improvement of the SNR by application of a matched filter: (a) raw FID signal; (b) FT of the raw FID signal; (c) FID signal after application of a matched filter; (d) FT of the filtered FID.

The sign $\mp$ is determined by the sign of α_1, given by $\alpha_1 = [(a_r/T^*_{2_1}) - (b/a_r)]$.

Choosing a very large value of the translation parameter b, for example, b_0 ($b_0 > b_r$), allows computation of the φ_1 value from the phase of Eq. [32]. To estimate the values of A_1 and $T^*_{2_1}$, the modulus is stored on M points and fitted to its expression in Eq. [32] by a nonlinear-regression algorithm. Unfortunately, it is difficult to determine the number M, which decreases when the value of b_r, which is connected to the unknown value of $T^*_{2_2}$, increases. Furthermore, to have an accurate estimate, the number M should be as large as possible, which is not generally the case if $T^*_{2_2}$ is close to $T^*_{2_1}$, even if the value of $T^*_{2_2}$ is known. To solve this problem, the first component must be separated from the signal. The interactions between the components are to be investigated from their frequency difference or from their amplitude ratio. Here we observe the frequency difference, because it is easier to obtain. Two situations must be considered.

(1) If the frequencies of the two components are sufficiently far away from each other, the fast decay of $\hat{g}$ will allow us to treat the first component independently of the second. The interactions between the components are practically nonexistent, and their corresponding $Z_a(b)e^{i\Theta_a(b)}$ quantity in Eq. [28] is zero. $S_{a_r}(b)$ of Eq. [32] becomes valid for every point b, allowing estimation of the values of A_1 and $T^*_{2_1}$ from the modulus and separation of the first component from the signal.

(2) As for overlapping resonances, if the difference between the two frequencies is small the quantity $Z_a(b)e^{i\Theta_a(b)}$ is not zero. This prevents us from treating the first component independently from the second. The values of A_1 and $T^*_{2_1}$ are estimated according to the contribution of the second component. The full WT, $S_a(b)$, of Eq. [28] should be computed for $a = a_r$. As a function of the a_r value involving $\Delta_1 = 0$ and $C1 = 0$ for the phase $\Phi 1_{a_r}(b)$ in Eq. [30], $\Theta_{a_r}(b)$ becomes

$$\Theta_{a_r}(b) = (\omega_2 - \omega_1)b + (\varphi_2 - \varphi_1) - \frac{a_r\Delta_2}{T^*_{2_2}} + \operatorname{Arctg}\left(\frac{C2_{a_r}(b)}{B2_{a_r}(b)}\right). \quad [33]$$

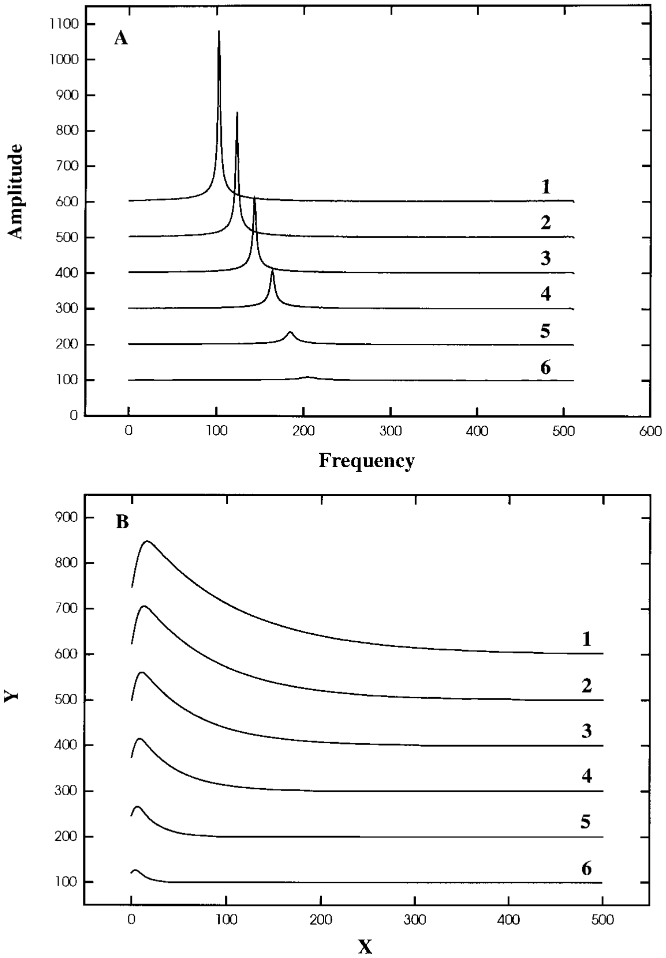

FIG. 6. (A) Spectra of simulated signals (1–6), each composed of one resonance. (B) The moduli of the WT of the signals.

The dominant term in Eq. [33] is $(\omega_2 - \omega_1)b$. Referring to (*17*), and due to the small difference between ω_1 and ω_2, the values of the other terms may be neglected. $\Theta_{a_r}(b)$ is approximated by

$$\Theta_{a_r}(b) \approx (\omega_2 - \omega_1)b. \qquad [34]$$

Substituting $\Theta_{a_r}(b)$ in Eq. [28], $S_{a_r}(b)$ is approximated by

$$S_{a_r}(b) \approx |S1_{a_r}(b)| \times \sqrt{1 + Z^2_{a_r}(b) + 2Z_{a_r}(b)\cos[(\omega_1 - \omega_2)b]} \times e^{i[\Phi 1_{a_r}(b) + \Psi_{a_r}(b)]}, \qquad [35]$$

with $\Psi_{a_r}(b) = \mathrm{Arctg}[R_{a_r}(b)/T_{a_r}(b)]$, where $R_{a_r}(b) = Z_{a_r}(b)\sin[(\omega_2 - \omega_1)b]$ and $T_{a_r}(b) = 1 + Z_{a_r}(b)\cos[(\omega_2 - \omega_1)b]$.

Application of the nonlinear regression algorithm to the modulus of Eq. [35] allows us to estimate not only the values of A_1 and $T^*_{2_1}$, but also the parameter values of A_2, $T^*_{2_2}$, and ω_2 of the contributing second component s_2 in $S_{a_r}(b)$. Here the estimated value of A_2 represents the contribution of the second component in $S_{a_r}(b)$, and not the total amplitude resonance of s_2 in the signal $s(t)$. If ω_2 is far from ω_1, s_2 contributes little to $S_{a_r}(b)$, and its estimated A_2 value is small compared with the total amplitude resonance of s_2. Inversely, if ω_2 is close to ω_1 the estimated value of A_2 is larger.

To separate the first component s_1 from the signal, the terms $Z_{a_r}(b)$ and $\Psi_{a_r}(b)$ should be negligible in Eq. [35]. Note that the value of $Z_{a_r}(b)$, according to Eq. [29], is negligible if the value of A_2 is small compared with the value of A_1. The resolution enhancement of the wavelet in the frequency domain causes the wavelet $\hat{g}$ to decay faster. Its frequency band is narrowed and focused around the frequency of the first component. $S_{a_r}(b)$ is smoothed, containing mainly the first component, and the influence of the second component is reduced. Thus component s_1 may be separated and filtered from the signal $s(t)$. The more the frequency resolution of the wavelet is enhanced, the more the contribution of the second component is attenuated. The enhancement of the frequency resolution of the wavelet is limited by the signal duration. The contribution of the wavelet in the time domain becomes wider.

The procedure in practice is outlined in Fig. 4: The values of a_r and ω_0 are multiplied by a given positive factor f ($f > 1$) to enhance the frequency resolution of the wavelet and keep its central frequency constant ($\Delta_1 = 0 \Rightarrow \omega_1 = f\omega_0/fa_r$). The smoothed $S_{fa_r}(b)$ is computed. The values of A_1, $T^*_{2_1}$, A_2, $T^*_{2_2}$, and ω_2 are estimated from the modulus of Eq. [35]. A_1 is compared with A_2, and if the condition $|A_2/A_1| < \epsilon$ is fulfilled, the procedure stops. Otherwise, the factor f is increased and a new iteration begins by executing the same steps as above. At convergence of this procedure, the final estimated value of A_2 is small compared with the value of A_1. The terms $Z_{fa_r}(b)$ and $\Psi_{fa_r}(b)$ become negligible in Eq. [35] and $S_{fa_r}(b)$ may be approximated by

$$S_{fa_r}(b) \approx \left| \sqrt{\frac{\pi}{2}}\, A_1 e^{\{[a_r^2/2(T^*_{2_1})^2] - b/T^*_{2_1}\}}[1 \mp (1 - e^{-\alpha_1^2})^{1/2}] \right| \times e^{i(\omega_1 b + \varphi_1)}. \qquad [36]$$

The WT described by Eq. [36] is equal to the first component s_1 of the signal at every point $t = b$ up to a known function $F_1(b)$ similar to Eq. [24]. The separated component is subtracted from the signal with respect to $F_1(b)$, and the second

TABLE 1
Estimated Values of the MRS Parameters Obtained by WT of Simulated FIDs with One Component

Signal	1	2	3	4	5	6
δ (normalized)	**0.100**	**0.120**	**0.140**	**0.160**	**0.180**	**0.200**
	0.100	0.120	0.139	0.159	0.179	0.200
T_2^* (ms)	**100**	**80**	**60**	**40**	**20**	**10**
	100.31	80.79	60.78	40.18	19.93	9.37
A (a.u.)	**120**	**100**	**80**	**60**	**40**	**20**
	118.21	98.76	79.02	59.33	39.89	21.00
φ (rad)	**0.17**	**0.15**	**0.13**	**0.11**	**0.09**	**0.07**
	0.19	0.14	0.12	0.10	0.08	0.05
a_r	8.75	7.29	6.25	5.47	4.86	4.37
b_0	500	450	400	350	250	100
j	9	10	9	12	14	16

Note. The reference values are in bold-face type. Figure 6A displays the spectra of the signals. a_r indicates the value of the dilation parameter of the wavelet at the convergence of the first iterative procedure. b_0 is the point estimation of the signal frequency. The required number of iterations is noted by j.

component of the signal is quantified using only the iterative procedure in Fig. 2.

This development may be extended on a FID signal containing more than two components. The proposed solutions are included in a third iterative procedure. The number of iterations of this third procedure will be equal to the number of signal components. At each iteration, the frequency of the longest-time component among the remaining components in the signal is detected. The effects of the component interactions are reduced, and the isolated component is quantified and extracted from the raw signal.

Case of a Noisy Signal

The random noise encountered in the FID signal originates largely from thermal noise in the probe and early stages of the receiver during data acquisition. The FID decays with time, while the noise amplitude remains constant. In some cases, the amplitude of noise is important and may complicate detection of the resonances.

An efficient method for increasing the SNR consists in multiplying the data by a decreasing exponential function, written as

$$f(t) = e^{(-t/T)}, \qquad [37]$$

where $T > 0$ is the constant time of the window function $f(t)$. The desired reduction in the size of the tail of the signal occurs, and sensitivity is enhanced by using this filter. Multiplication in this fashion speeds up the apparent decay of the signal, given by

TABLE 2
Values of the MRS Parameters Estimated by WT on a Simulated Data Set Containing Two Overlapping Resonances

Signal	A		B		C	
Peak number	1	2	1	2	1	2
δ (normalized)	**0.172**	**0.160**	**0.160**	**0.175**	**0.200**	**0.250**
	0.170	0.158	0.158	0.176	0.199	0.249
T_2^* (ms)	**75**	**70**	**50**	**10**	**7**	**5**
	77.11	71.84	49.01	11.12	7.54	4.75
A (a.u.)	**50**	**55**	**125**	**150**	**80**	**70**
	46.32	52.66	130.81	134.93	84.58	67.18
φ (rad)	**0.20**	**0.10**	**0.15**	**0.25**	**0.40**	**0.30**
	0.18	0.11	0.17	0.22	0.42	0.28
a_r	32.03	10.89	15.99	10.08	8.84	7.84
b_0	300	250	150	75	35	20
j	29	7	13	7	10	9

Note. The reference values are in bold-face type. The spectra of the signals A, B and C are shown in Figs. 7A, 7C, and 7D respectively. j is the number of iterations of the first and second iterative procedures. For the signal C, only the first iterative procedure was used.

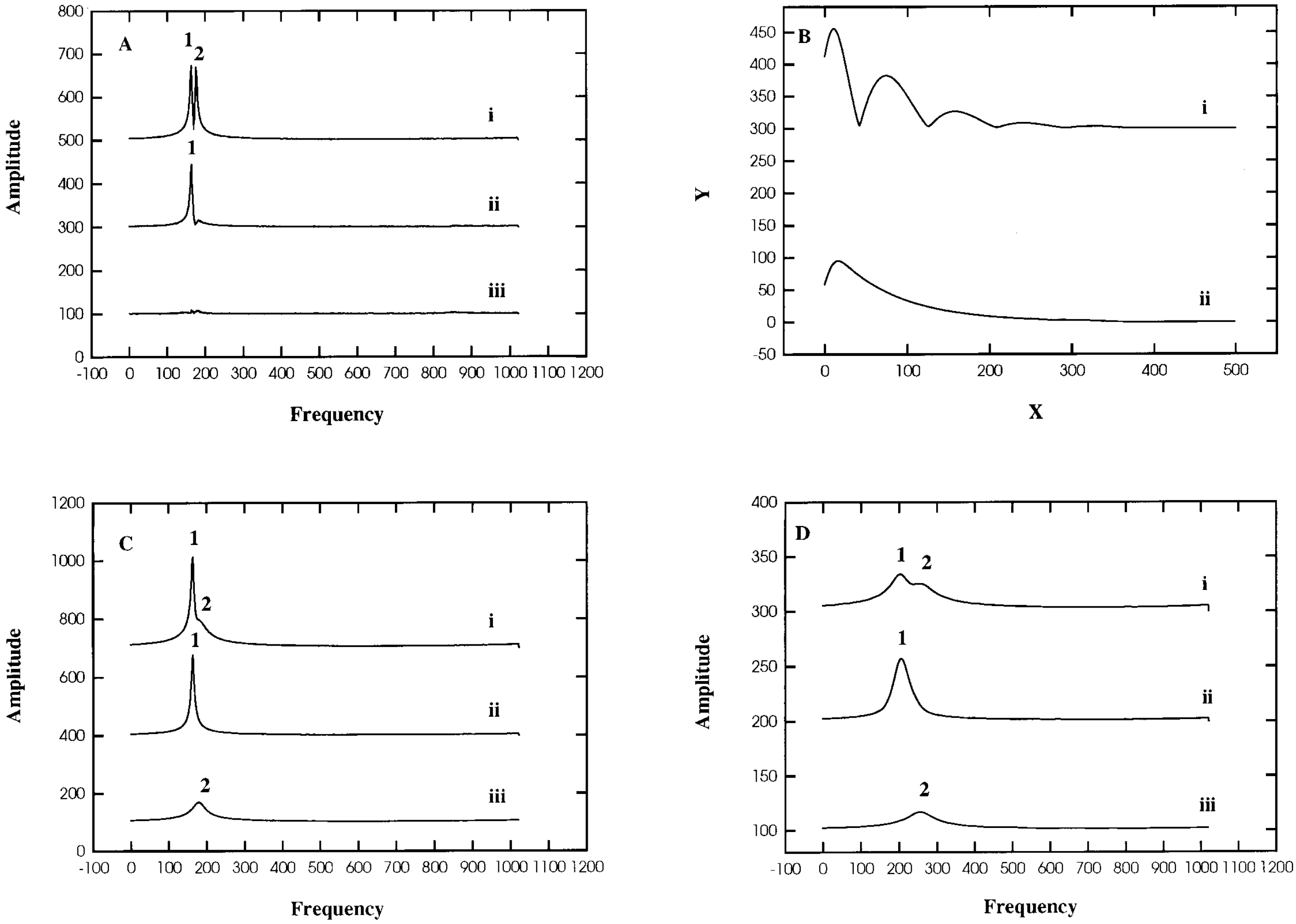

FIG. 7. (A). (i) Spectrum of the simulated signal (A) composed of two resonances (1 + 2). (ii) Spectrum of the residue signal after subtraction of the first component (1). (iii) Spectrum of the final residue after subtraction of the second component (2). (B). (i) Shape of the modulus of the WT associated to the first separated component (1) of the signal (A) after the first iterative procedure convergence. (ii) Shape of the same modulus after the second iterative procedure convergence. The effect of the second component (2) is reduced in S_{fa_r} (b). (C). (i) Spectrum of the signal (B). (ii) WT spectrum of the separated first component (1). (iii) WT spectrum of the second component (2). (D). (i) Spectrum of the simulated signal (C). (ii) WT spectrum of the first component (1). (iii) WT spectrum associated to the remaining component in the signal.

$$\frac{1}{T_2^a} = \frac{1}{T_2^*} + \frac{1}{T}. \quad [38]$$

The estimation of the frequency components at the end of the signal is still possible by using the first iterative procedure (see Fig. 5), and according to the frequency difference between the components, the second iterative procedure is used to estimate A and T_2^* values. To recover the values of the apparent relaxation time, the following relation is used:

$$\frac{1}{T_2^*} = \frac{1}{T_2^a} - \frac{1}{T}. \quad [39]$$

APPLICATION TO SIMULATED MRS DATA

To test the accuracy and the efficiency of the proposed quantification technique, FIDs were simulated by PC software according to Eq. [7] and were quantified by WT. The sampling frequency was normalized to 1. Each simulated signal was stored on 1024 points. To have an accurate estimate of A and T_2^* values, the order of the series U_k of the terms $B2$ and $C2$ contained in $|S2_{a_r}(b)|$ was chosen to be 10. The start value of the analyzing frequency ω_0 of the wavelet was chosen as greater than 5 and was set to 11. The initial values of the dilation parameter a_0 and the factor f were taken as 1 and 2, respectively. The precision order of the two iterative procedures was ensured by the value of ϵ set to 0.001. The estimated and reference MRS parameter values, the chosen value of b_0, the value of a_r obtained after convergence of the iterative procedures, and the requested number of iterations, noted j, for each signal component are reported in Tables 1, 2, and 3.

Case of a Signal with a Single Component

The aim of this first simple test was to investigate the behavior of the WT quantification method and to check the

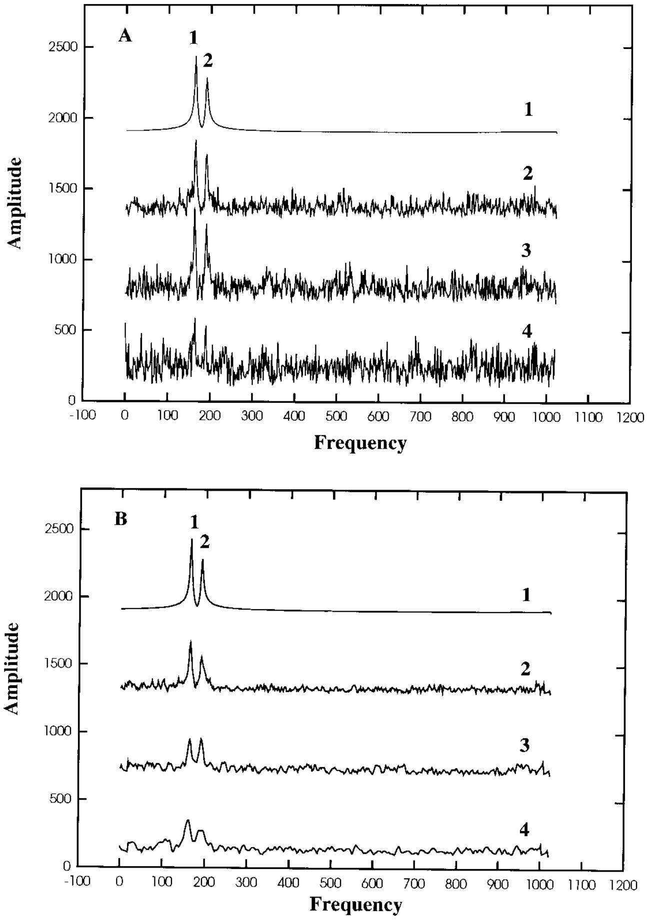

FIG. 8. (A) Spectra of the simulated noisy FIDs (1–4) composed of two resonances with $\sigma_n = 0$, 200, 300, and 400 respectively. (B) Spectra of the signals after noise reduction, using the low-pass filter on the signals (2, 3, and 4), with different time constant values T equal to 145, 80, and 50 ms, respectively.

number of requested iterations. Six simulated signals, each containing one component, were quantified (Fig. 6A). For each signal, the translation parameter point b_0 was chosen and the first iterative procedure was applied. This procedure converged and stopped at the final value a_r, fulfilling Eq. [22]. The frequency of the signal and its phase were estimated, and the nonlinear analysis algorithm was used to fit the modulus to its expression and to give the values of A and T_2^* (Fig. 6B). The results obtained are reported in Table 1.

Case of Two Overlapping Resonances

This situation is often encountered in biomedical MRS, for instance, in the *in vitro* high-resolution ^{1}H MRS of body fluids or in *in vivo* ^{31}P MRS of brain tissue. Three simulated signals (A, B, and C) each composed of two overlapping resonances, were quantified. The results obtained are reported in Table 2. For the first signal (Fig. 7A), the first iterative procedure was applied. The translation parameter point b_0 was set to 300. We assumed that for $b \geqslant 300$, the remaining resonance in the signal is the longest one (say, the first one). At the convergence of the procedure, the linear parameter values $\omega_1(\delta_1)$ and φ_1 of the first component were estimated. The second iterative procedure was used to estimate the parameter values of A_1 and $T_{2_1}^*$ of the localized first component and to separate that component from the signal. The iteration stopped when the estimated value of A_2 reached 0.08, which satisfies the condition $|A_2/A_1| < \epsilon$. The number of iterations of this second procedure depends on the extent of the component interactions. For this example, the procedure stopped at the 20th frequency wavelet enhancement ($f = 20$). Note that at each iteration, the estimated values of A_1, $T_{2_1}^*$, and $T_{2_2}^*$ varied little, whereas the estimated value of A_2 decreased. This demonstrates that the contribution of the second component was reduced when the frequency resolution of the wavelet was enhanced. The change in shape of the modulus of the first component, shown in Fig. 7B, after the application of the second procedure is another confirmation of this assumption. The first separated component was filtered from the signal, and the parameter values of the second component were estimated using only the first iterative procedure.

In signal B (Fig. 7C), the aim was to extract a narrow peak from a broad baseline containing a large peak (a short T_2^* value). The same steps as used previously were repeated. The translation parameter point b_0 was chosen equal to 150. The longest-time component was first quantified and subtracted from the raw signal by applying the first and second procedures, respectively. The second procedure took more time to converge ($f = 6$) because of the small difference in frequency between the components and the large value of the amplitude resonance A_2. After subtraction of the first component from the signal, the second component was quantified by applying only the first iterative procedure (Fig. 7C).

In the last example (Fig. 7D), the resonances were large and had amplitudes and T_2^* values close to each other. This test illustrates the capacity of the WT method to separate two large resonances as in the ^{1}H MRS signal of the alkyl region of the plasma lipoprotein. For this example, the frequency difference between the two components was large enough so that the first iterative procedure alone gave satisfactory quantification of the two resonances.

Case of a Noisy Signal

The low-pass filter was introduced in this test to obtain a satisfactory SNR in order that the quantification procedures would remain valid. A noise-free signal, containing two components and three similar signals with additive complex noise, with noise variance σ_n equal to 200, 300, and 400 respectively, was simulated (Fig. 8A). The injected noise in the signals is white and uniform. The low-pass filter was

TABLE 3
Case of Noisy Signals Containing Two Components

Signal	$\sigma_n = 0$ (1)		$\sigma_n = 200$ (2)		$\sigma_n = 300$ (3)		$\sigma_n = 400$ (4)	
T (ms)	—		145		80		50	
Peak	1	2	1	2	1	2	1	2
δ (normalized)	**0.160**	**0.185**	**0.160**	**0.185**	**0.160**	**0.185**	**0.160**	**0.185**
	0.158	0.185	0.156	0.184	0.159	0.186	0.158	0.186
$^{\#}T_2^*$ (ms)	**80**	**70**	**80**	**70**	**80**	**70**	**80**	**70**
	81.50	69.25	82.17	72.47	81.20	76.13	73.60	61.42
A (a.u.)	**150**	**120**	**150**	**120**	**150**	**120**	**150**	**120**
	147.72	118.15	154.64	124.85	143.82	115.56	127.13	106.24
φ (rad)	**0.21**	**0.14**	**0.21**	**0.14**	**0.21**	**0.14**	**0.21**	**0.14**
	0.23	0.12	0.20	0.13	0.22	0.11	0.23	0.11
$\Diamond T_2^*$ (ms)	—	—	52.45	48.32	40.30	39.01	29.77	26.06
a_r	15.98	9.47	19.90	14.03	17.73	20.04	16.98	16.02
b_0	300	250	150	100	135	120	50	30
j	14	8	25	12	21	18	17	14

Note. The WT estimated values are compared with the reference values in bold-face type. The spectra of the processed signals 1, 2, 3, and 4 are shown in Fig. 8B. They were obtained by application of the low-pass filter with different values of constant time T on the signals. The sign $\Diamond$ denotes the T_2^* values obtained by the regression analysis algorithm applied to the modulus. The sign # denotes the recovered T_2^* values obtained after using Eq. [39]. j indicates the number of iterations including the second and/or the first iterative procedures.

first applied on each signal to enhance the SNR with filter time constant T equal to 145, 80, and 50 ms, respectively (Fig. 8B). Due to the large difference between the frequencies of the two components in signals 1 and 2, only the first iterative procedure was used to quantify the components. For signals 3 and 4, the components became large and overlapped in the frequency domain. To separate them, the second iterative procedure was needed. The MRS parameter values of the two components were estimated for each signal and given in Table 3.

The correlation coefficients between reference values of δ, A, and T_2^*, and the corresponding WT estimations were calculated on the 20 simulated resonances: 6 sets of data with one resonances (Table 1, Fig. 6), 3 sets of data with two overlapping resonances (Table 2, Fig. 7), and 4 sets of data with two resonances and varying noise levels (Table 3, Fig. 8). The correlation coefficients are 0.985, 0.999, and 0.989 for A, δ, and T_2^*, respectively. The noise level appeared to be the most disturbing factor, with more effect on A and T_2^* than on δ (Fig. 9).

APPLICATION TO REAL BIOMEDICAL MRS DATA

In order to further demonstrate the usefulness of the WT method in biomedical MRS, a selected example is presented. In this example, a set of FIDs resulting from a ^{31}P MRS experiment on perfused working smooth muscle was considered. The set contains six peaks: phosphomonoesters (PME); inorganic phosphates (Pi), phosphocreatine, a common reference peak at 0 ppm (PCr), and γ, α, and β ATP

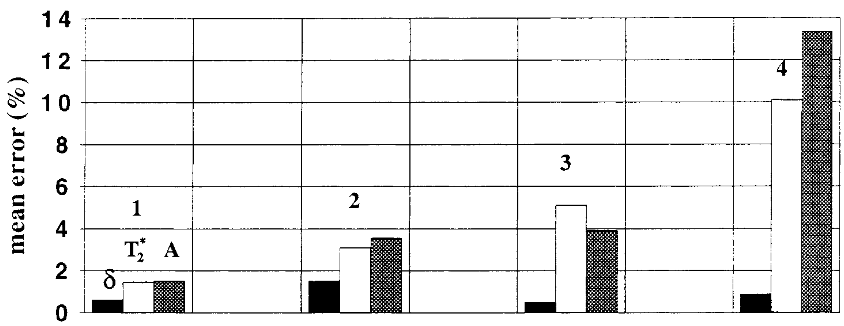

FIG. 9. Mean error (in %) in WT estimated parameters δ, A, and T_2^* in relation to signal noise level. (1) Noise-free signal, (2) $\sigma_n = 200$, (3) $\sigma_n = 300$, and (4) $\sigma_n = 400$.

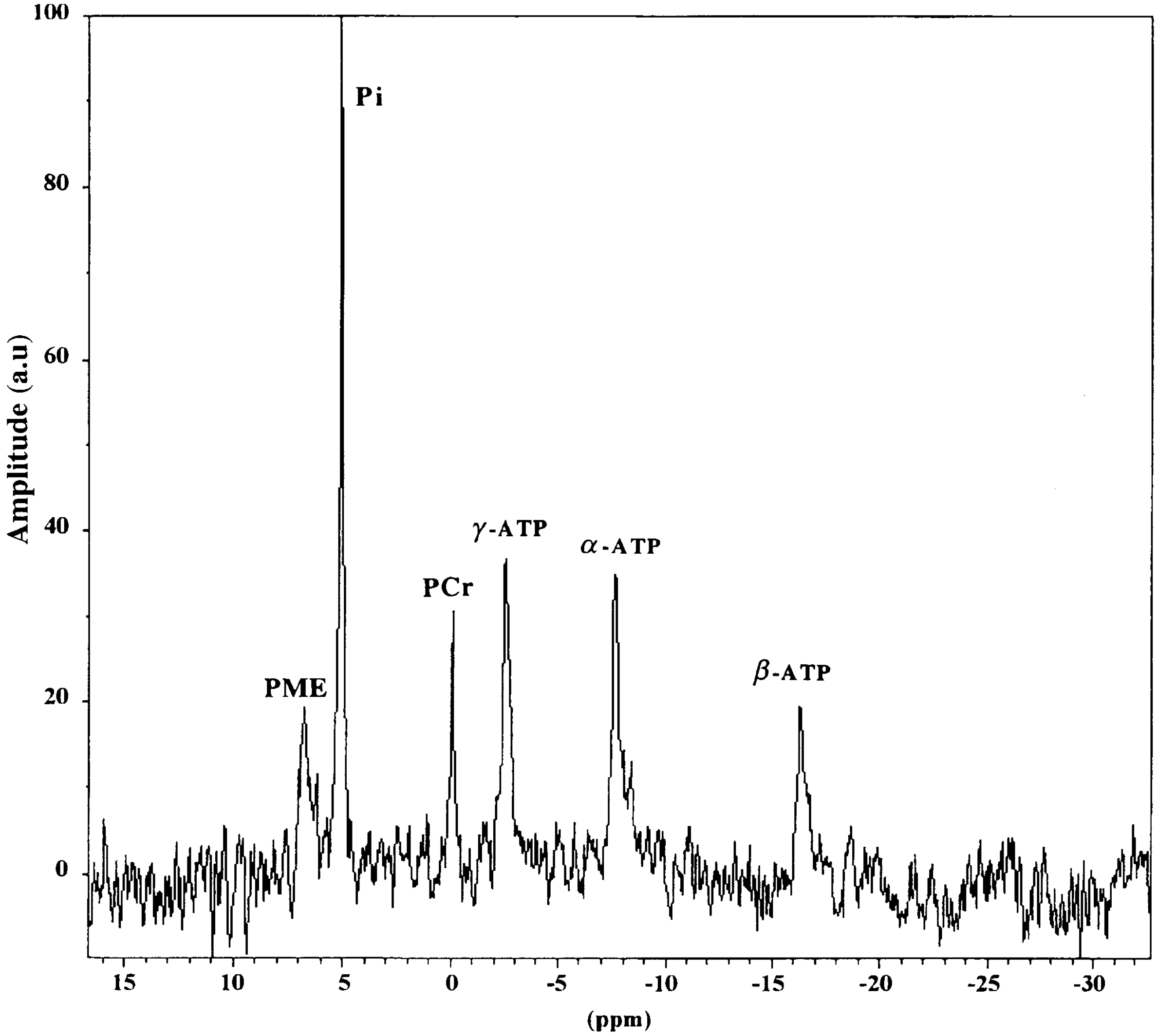

FIG. 10. Phase-corrected ^{31}P spectrum of a perfused working rat smooth muscle (202.45 MHz, 14.5 μs pulse, 1200 scans, $\pm$5000 Hz spectral width, and 32K data points).

(adenosine triphosphate). The ^{31}P MRS was performed at 202.45 MHz on an Avance DMX500 Spectrometer (Bruker, Wissenbourg, France). FIDs were acquired with a 14.5 μs pulse, 1200 accumulations, a $\pm$5000 Hz spectral width, and 32 K data points. A 20 Hz line broadening was applied before processing data to enhance the SNR. Figure 10 shows the corresponding spectrum.

The results obtained by WT (Table 4) were compared to those obtained by a Bruker spectral-fitting method (UXNMR 1D, Bruker) and a time-domain method called variable-projection method (VARPRO) (*21, 22*). Only the first 1024 FID points were processed by both WT and VARPRO, whereas the spectral-fitting method fitted all the data points to a Lorentzian model. Unlike the other two methods, WT did not require baseline or phase corrections nor any prior knowledge before quantification.

CONCLUSION

A quantification method based on wavelet-transform analysis has been proposed. Described by two iterative procedures and a nonlinear regression analysis algorithm, the technique presented is a combination of linear and nonlinear methods. As an alternative method to the Fourier transform, the wavelet transform appears efficient in obtaining accurate estimates of the values of the MRS parameters δ, T_2^*, A, and φ of each signal component.

The mathematical development shows the role of the apparent relaxation time T_2^* in estimating the chemical shift. The first iterative procedure, utilizing the information obtained from the phase of the wavelet signal representation, successfully achieves this operation. Extraction of the components from the signal depends on component interactions.

TABLE 4
Comparison of Results Obtained by Spectral Fitting, Variable-Projection Method (VARPRO), and Wavelet Transform

Spectral fitting			VARPRO			Wavelet transform		
δ (ppm)	T_2^* (ms)	A (a.u)	δ (ppm)	T_2^* (ms)	A (a.u)	δ (ppm)	T_2^* (ms)	A (a.u)
6.816	4.44	430.241	6.817	3.29	496.478	6.816	3.35	497.963
5.083	8.81	1120.204	5.177	8.77	1012.271	5.087	9.07	991.521
−0.105	9.29	312.281	0.003	8.60	313.983	−0.095	8.83	310.039
−2.514	4.55	821.693	−2.437	4.28	804.251	−2.499	4.21	796.228
−7.603	5.00	710.213	−7.511	4.60	679.721	−7.577	4.63	683.175
−16.274	3.80	559.196	−16.149	3.43	567.434	−16.253	3.45	557.750

Note. Phase values were not estimated. VARPRO software fixed them to a constant value, whereas the spectral-fitting program did not estimate them.

We have shown that the amplitude ratio and the frequency difference between the components determine their degree of interaction. The second iterative procedure proposed manipulates the frequency content of the WT by using wavelet properties and reduces the effect of the component interactions. Moreover, by investigating the FID signal in the time-frequency domain, the major quantification problems in biomedical MRS, such as overlapping resonances, are addressed.

A poor signal-to-noise ratio may hinder this operation, but since, as shown here, the MRS parameter values of a previously known number of components of the FID signal can be computed, the proposed classical solution is sufficient to reduce noise in the data. The quantification procedures remain valid, and the changes in the apparent relaxation time values from application of the low-pass filter are compensated.

The practical examples presented show that the method is suitable for different kinds of FID signals with their specific problems. Results obtained to date demonstrate the estimation accuracy of the WT method. Computation time depends on the complexity of the signal, on the number of components, and obviously on the computer power, and may be reduced if the components do not overlap.

APPENDIX 1

This Appendix provides the computation of the integral $I = \int_\alpha^\infty e^{[(-t^2/2)+i\Delta t]}dt$, where $\alpha = [(a/T_2^*) - (\mathrm{b/a})]$. I may be written as

$$I = \int_0^\infty e^{[(-t^2/2)+i\Delta t]}dt - \int_0^\alpha e^{[(-t^2/2)+i\Delta t]}dt$$
$$= I_1 - I_2 \ \forall\alpha. \qquad [40]$$

Considering the rectangle (OABC),

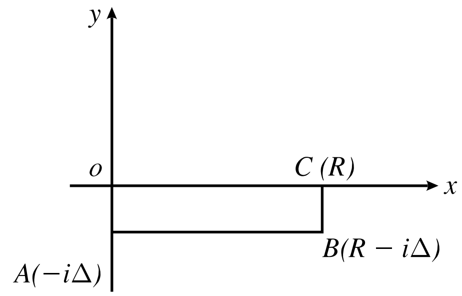

,

let $f(z)$ be a complex function under this rectangle, given by $f(z) = e^{-z^2/2}$, where $z = t - i\Delta$, and t runs from 0 to ∞. I_1 may be written as

$$I_1 = e^{-\Delta^2/2}\int_{-\mathrm{i}\Delta}^{\infty-\mathrm{i}\Delta} e^{-z^2/2}dz. \qquad [41]$$

The function $z \to e^{(-z^2/2)}$ is analytical on and inside the rectangle OABCO. Using the Cauchy theorem, we have

$$\oint_{OABCO} f(z)dz = \int_{OA} e^{-z^2/2}dz + \int_{AB} e^{-z^2/2}dz + \int_{BC} e^{-z^2/2}dz + \int_{CO} e^{-z^2/2}dz = 0. \qquad [42]$$

(1) On the segment OA of the rectangle, $z = -iy$, where y runs from 0 to Δ. Using the polar co-ordinates ($r \in [0, \sqrt{2}\Delta]$, $\theta \in [0, \pi/2]$) and the sign of Δ, $f(z)$ is given by

$$\int_{OA} e^{-z^2/2}dz = \int_0^\Delta - ie^{y^2/2}dy$$
$$\approx \mp\mathrm{i}\left[\frac{\pi}{2}(e^{\Delta^2} - 1)\right]^{1/2}. \qquad [43]$$

(2) On the segment AB, $z = x - i\Delta$, $x \in [0, R]$, so that

$$\int_{AB} e^{-z^2/2} dz = \int_{-i\Delta}^{R-i\Delta} e^{-(x-i\Delta)^2/2} dx. \quad [44]$$

Equation [44] is equal to I_1 up to the term $e^{-\Delta^2/2}$.

(3) On the segment BC, $z = R - iy$ and $y \in [\Delta, 0]$. Thus,

$$\int_{BC} e^{(-z^2/2)} dz = -i \int_{\Delta}^{0} e^{-(R-iy)^2/2} dy$$
$$= -ie^{-R^2/2} \int_{\Delta}^{0} e^{(y^2/2 + iRy)} dy. \quad [45]$$

Equation [45] may be estimated in the limit by

$$\int_{BC} f(z) dz \leqslant -ie^{-R^2/2} \int_{\Delta}^{0} e^{y^2/2} dy. \quad [46]$$

The integral $\int_{\Delta}^{0} e^{y^2/2}$dy has a finite value; hence, Eq. [46] decrease to zero when $R \to \infty$.

(4) On segment CO, $z = x$, with $x \in [R, 0]$. Using the polar co-ordinates ($r \in [0, \sqrt{2}\Delta]$, $\theta \in [0, \pi/2]$), we obtain

$$\int_{CO} e^{-z^2/2} dz = -\int_{0}^{R} e^{-x^2/2} dx$$
$$\approx -\left[\sqrt{\frac{\pi}{2}}\,(1 - e^{-R^2})\right]^{1/2}. \quad [47]$$

Equation [47] approaches $-\sqrt{\pi/2}$ when $R \to \infty$.

Substituting the values of Eqs. [43], [44], [46], and [47] into Eq. [42], we obtain

$$I_1 \approx \begin{cases} \sqrt{\frac{\pi}{2}}\, e^{-\Delta^2/2}[1 + i\sqrt{e^{\Delta^2} - 1}] \text{ if } \Delta > 0 \\ \sqrt{\frac{\pi}{2}}\, e^{-\Delta^2/2}[1 - i\sqrt{e^{\Delta^2} - 1}] \text{ if } \Delta < 0 \end{cases}. \quad [48]$$

For $I_2 = \int_0^{\alpha} e^{-t^2/2} e^{i\Delta t} dt$, we use the Taylor series expansion of the term $e^{i\Delta t}$.

$$I_2 = \int_0^{\alpha} \left[\sum_{k=0}^{\infty} \frac{(i\Delta t)^k}{k!}\right] e^{-t^2/2} dt$$
$$= \sum_{k=0}^{\infty} \frac{(i\Delta)^k}{k!} \int_0^{\alpha} t^k e^{-t^2/2} dt$$
$$= \sum_{k=0}^{\infty} \frac{(i\Delta)^k}{k!}\, U_k, \quad [49]$$

where $U_k = \int_0^{\alpha} t^k \mathrm{e}^{-t^2/2} dt$. If $k = 0$ and the polar co-ordinates are used:

$$U_0 = \int_0^{\alpha} e^{-t^2/2} dt \approx \begin{cases} \sqrt{\frac{\pi}{2}}\, \sqrt{1 - e^{-\alpha^2}} \text{ if } \alpha > 0 \\ -\sqrt{\frac{\pi}{2}}\, \sqrt{1 - e^{-\alpha^2}} \text{ if } \alpha < 0 \end{cases}.$$

If $k = 1$, by changing variables, we obtain $U_1 = \int_0^{\alpha} te^{-t^2/2} dt = [1 - e^{-\alpha^2/2}]$. The general term for this series for $k \geqslant 2$, is given by

$$U_k = \int_0^{\alpha} t^k e^{-t^2/2} dt$$
$$= -\int_0^{\alpha} t^{k-1} (e^{-t^2/2})'\, dt$$
$$= -\alpha^{k-1} e^{-\alpha^2/2} + (k-1) \int_0^{\alpha} t^{k-2} e^{-t^2/2} dt$$
$$= -\alpha^{k-1} e^{-\alpha^2/2} + (k-1) U_{k-2}. \quad [50]$$

The series $\Sigma_{k=0}^{\infty} [(i\Delta)^k/k!] U_k$ is recurrent and convergent. By combining Eqs. [40], [48], and [49], I is approximated as

$$I \approx \left[\sqrt{\frac{\pi}{2}}\, e^{-\Delta^2/2}(1 \pm i\sqrt{e^{\Delta^2} - 1})\right]$$
$$- \sum_{k=0}^{\infty} \frac{(i\Delta)^k}{k!}\, U_k \ \forall \alpha. \quad [51]$$

Equation [51] may be described by $I = [B + iC]$, where B is

$$B = \sqrt{\frac{\pi}{2}}\, e^{-\Delta^2/2} \mp \sqrt{\frac{\pi}{2}}\, \sqrt{1 - e^{-\alpha^2}}$$
$$- \sum_{k=2}^{\infty} \frac{(i\Delta)^k}{k!}\, U_k \ (k \text{ pair}) \quad [52]$$

and

$$C = \pm\sqrt{\frac{\pi}{2}}\, e^{-\Delta^2/2}(\sqrt{e^{\Delta^2} - 1}) - \Delta(1 - e^{-\alpha^2/2})$$
$$- \sum_{k=2}^{\infty} \frac{(i\Delta)^k}{k!}\, U_k \ (k \text{ odd}). \quad [53]$$

The signs $\mp$ and $\pm$ are determined by the signs of α and Δ respectively. Note that the term C is zero if $\Delta = 0$. If we restrict k to unity, B, and C become

$$B = \sqrt{\frac{\pi}{2}}\, e^{-\Delta^2/2} \mp \sqrt{\frac{\pi}{2}}\, \sqrt{1 - e^{-\alpha^2}} \text{ and}$$

$$C = \pm\sqrt{\frac{\pi}{2}}\, e^{-\Delta^2/2}(\sqrt{e^{\Delta^2}} - 1) - \Delta(1 - e^{-\alpha^2/2}).$$

APPENDIX 2

In this Appendix, we investigate the term $d[\text{arctag } C/B)]/db$. If we restrict the series U_k to its first two terms $(k = 1)$, we obtain

$$\text{arctag}\left(\frac{C}{B}\right) = \text{arctg}\left[\frac{\pm\sqrt{\pi/2}\, e^{-\Delta^2/2}(\sqrt{e^{\Delta^2}} - 1) - \Delta(1 - e^{-\alpha^2/2})}{\sqrt{\pi/2}\, e^{-\Delta^2/2} \mp \sqrt{\pi/2}\, \sqrt{1 - e^{-\alpha^2}}}\right]. \quad [54]$$

Writing $d[\text{arctg}(C/B)]/db$ as a function of α $[\alpha = (a/T_2^*) - (b/a)]$, we obtain

$$\frac{d[\text{arctg}(C/B)]}{db} = \frac{e^{-\alpha^2/2}\left[\frac{\Delta}{a}\alpha B - C\left(\pm\frac{1}{a}\sqrt{\pi/2}\,\alpha e^{-\alpha^2/2}\sqrt{1 - e^{-\alpha^2}}\right)\right]}{B^2 + C^2}. \quad [55]$$

The denominator of Eq. [55] is not zero. The term

$$\frac{\Delta}{a}\alpha B - C\left[\pm\frac{1}{a}\sqrt{\frac{\pi}{2}}\,\alpha e^{-\alpha^2/2}\,\sqrt{1 - e^{-\alpha^2}}\right]$$

has a finite value, which is zero if $\Delta = 0$. The numerator of Eq. [55] approaches zero as the value of $|\alpha|$ becomes larger. For values of b larger than b_r, the factor $e^{(-\alpha^2/2)}$ is negligible, so that the function in Eq. [55] is zero.

ACKNOWLEDGMENTS

This work has been supported by a grant from Bruker Spectrospin S.A. (Wissenbourg, France), by a ''Programme Hospitalier de Recherche Clinique'' from the French Ministry of Health, and by a E.U. Biomed programme.

REFERENCES

1. A. Grossmann and J. Morlet, *Siam. J. Math. Anal.* **15,** 723 (1984).
2. H. Barkhuijsen, R. de Beer, and D. van Ormondt, *J. Magn. Reson.* **73,** 553 (1987).
3. J. C. Hoch, *Methods Enzymol.* **176,** 216 (1989).
4. R. de Beer and D. van Ormondt, *in* ''NMR Basic Principles and Progress,'' Vol. 26, p. 201, Springer-Verlag, Berlin 1992.
5. A. Diop, Y. Zaimwadghiri, A. Briguet, and D. Graveron-Demilly, *J. Magn. Reson. B* **105,** 17 (1994).
6. A. Grossmann, R. Kronland-Martinet, and J. Morlet, *in* ''Wavelets'' (J. M. Combes, A. Grossmann, and Ph. Tchamitchian, Eds.), p. 1, Springer-Verlag, Marseille, 1987.
7. P. Guillemain, R. Kronland-Martinet, and B. Martens, *in* ''Wavelets and Applications'' (Y. Meyer, Ed.), p. 39, Masson, Marseille, 1989.
8. D. S. Stephenson, *Prog. NMR Spectrosc.* **20,** 515 (1988).
9. N. Delprat, B. Escudie, Ph. Guillemain, R. Kronland-Martinet, Ph. Tchamitchian, and B. Torresani, *IEEE. Trans. Inform. Thoery* **38,** 644 (1992).
10. S. Mallat and W. L. Hwang, *IEEE Trans. Info. Theory* **38,** 617 (1992).
11. I. Daubechies, *IEEE Trans. Inform. Theory* **36,** 961 (1990).
12. S. L. Marple, *Proc. IEEE* **70,** 1238 (1982).
13. B. Torresani, *in* ''Wavelets and Applications'' (Y. Meyer, Ed.), p. 12, Springer-Verlag, Marseille, 1989.
14. D. W. Marquardt, *J. Soc. Indust. Appl. Math.* **11,** 431 (1963).
15. A. Vandenbos, *in* ''Handbook of Measurement Science'' (P. H. Sydenham, Ed.), Vol. 1, p. 331, Wiley, London, 1982.
16. A. Papoulis, ''Probability, Random Variables, and Stochastis Processes,'' Chap. 10, McGraw–Hill, New York, 1984.
17. J. C. Haselgrove, V. Harihara Subramanian, R. Christen, and J. S. Leigh, *Rev. Magn. Reson. Med.* **2,** 167 (1987).
18. A. E. Derome, ''Modern NMR Techniques for Chemistry Research,'' Organic Chemistry Series, Chap. 6, Pergamon Press, 1987.
19. J. H. J. Leclerc, *J. Magn. Reson.* **100,** 171 (1992).
20. S. L. Marple, ''Digital Spectral Analysis,'' Chap. 8, Prentice-Hall, Englewood Cliffs, New Jersey, 1987.
21. J. W. C. van der Veen, R. de Beer, P. R. Luyten, and D. van Ormondt, *Magn. Reson. Med.* **6,** 92 (1988).
22. A. Kinjn, R. de Beer, and D. van Ormondt, *J. Magn. Reson.* **97,** 444 (1992).